# Guidelines for Molybdenum Oxidation State and Geometry from X-Ray Absorption Spectroscopy at the Mo L 2,3 -edges

Alexy P Freitas, Rémi F André, Cyprien Poucin, Thi Kim-Chi Le, Jerick Imbao, Benedikt Lassalle-Kaiser, Sophie Carenco

**HAL Id: hal-03329787**
**https://hal.sorbonne-universite.fr/hal-03329787v1**

Submitted on 31 Aug 2021

# Guidelines for Molybdenum Oxidation State and Geometry from X-Ray Absorption Spectroscopy at the Mo L$_{2,3}$-edges

Alexy P. Freitas,[1] Rémi F. André,[1] Cyprien Poucin,[1] Thi Kim-Chi Le,[1] Jerick Imbao, [2] Benedikt Lassalle-Kaiser,[2,*] Sophie Carenco[1,*]

[1] Sorbonne Université, CNRS, Collège de France, Laboratoire de Chimie de la Matière Condensée de Paris, 4 place Jussieu, 75005 Paris, France

[2] Synchrotron SOLEIL, L'Orme des Merisiers, 91192 Saint-Aubin - BP 48, Gif-sur-Yvette Cedex, France.

\* Corresponding authors: sophie.carenco@sorbonne-universite.fr,

benedikt.lassalle@synchrotron-soleil.fr

**Abstract:** Molybdenum accepts oxidation states from –II to +VI. This versatility is highly beneficial for applications in catalysis, especially combined with sulfur to form the ubiquitous $MoS_2$ material. X-ray Absorption Near Edge Spectroscopy (XANES) is a particularly well-adapted technique to study simultaneously both elements, since the K-edge of S (2472 eV) and the $L_{2,3}$-edges of Mo (2520 - 2625 eV) have similar absorption energies. It provides information on both the electronic and local structure of metal-containing species and allows drawing structure-activity relationships. However, $L_{2,3}$-edges are difficult to interpret, especially for 4d and 5d transition metals. In addition, only few recent studies focus on the measurement of the signal of Mo-based reference compounds, meaning that the references from the literature do not benefit from recent technical progress. Notwithstanding theoretical tools that allow a deep understanding of such spectroscopic data, the lack of reference spectra prevents a quick yet reliable interpretation. In this work, we provide a method for the interpretation of X-ray absorption near edge structure (XANES) data at the Mo $L_{2,3}$-edges, based on a library of spectra of simple Mo compounds. From our analysis, we suggest using the $L_3$-edge to determine the oxidation state (in selected cases) and the $L_2$-edge to gain insight on geometry around the Mo atoms. This method is then applied to a series of molybdenum sulfides compounds in order to rationalize their structures. Besides this example, these guidelines should help to qualitatively interpret XANES of Mo at $L_{2,3}$-edges in future studies.

## 1. Introduction

Molybdenum can have any oxidation state ranging from -II to +VI and is a non-noble metal that forms a wide range of organometallic and inorganic compounds. As such, Mo is used for many applications in catalysis. As a first example, the ubiquitous $MoS_2$ compound is used for hydrodesulfurisation.[1,2] Interestingly, many examples in the literature show that the activity of molybdenum can be tuned by changing the environment of Mo in the catalyst. Molybdenum oxides catalyse oxidation of small organic molecules such as propane, butane or methane)[3–5], molybdenum sulfides catalyse the Hydrogen Evolution Reaction (HER)[6–11] and in living organisms, molybdenum nitrogenase is an enzyme known to catalyse the reduction of dinitrogen into ammonia.[12–14] In this context, optimising Mo catalysts towards a specific reactivity requires a precise knowledge of the local environment around the Mo atoms. Usual characterisation methods (powder X-ray diffraction, or electronic microscopy) cannot yield this information when Mo is only present as a minor species. On the contrary, X-ray Absorption Spectroscopy (XAS) is element-specific, so it is suitable to investigate precisely both the oxidation state of Mo and the symmetry around Mo atoms. Moreover, this technique allows performing *in situ* and/or *operando* experiments, thanks to the penetration depth of X-ray photons, albeit limited in the tender and soft X-ray ranges.

Although XAS is experimentally easier to perform at the K-edge of molybdenum (20 keV), this edge is not the best one to determine the oxidation state and symmetry of Mo atoms. On one hand, we know from crystal field theory that the symmetry around transition metals – such as Mo – is determined by the bonding of the valence d orbitals (4d for Mo) with the ligands. On the other hand, absorption at the K-edge depends on the probability for a 1s electron to transition to the empty valence p orbitals (5p for Mo). From the Laporte rule, the 1s → 4d transition is forbidden for symmetry reasons, so the 4d orbitals of Mo cannot be probed directly at the K-edge. This is particularly true for Mo in a centrosymmetric environment, such as octahedral. If the centre of inversion is lost, by distortion of the octahedron or switching to tetrahedral symmetry, hybridisation of the 4d orbitals with the 5p orbitals may lift the restriction, causing a pre-edge to appear. Despite this feature, using the pre-edge at the K-edge to determine precisely the geometry of Mo atoms remains limited by the absolute energy resolution (approximately 5 eV at the K-edge of Mo). Although High-Energy Resolution Fluorescence Detected XANES may overcome the resolution limit, this technique is only available in the Mo L-edges energy range at a very few beamlines. Instead,

accessing the geometry around Mo atoms by probing directly the 4d orbitals can be achieved at the $L_{2,3}$-edges.[5]

XANES at the $L_{2,3}$-edges solves both issues raised at the K-edge (sensitivity regarding symmetry and resolution). First, the valence d orbitals are probed directly since the electronic transition involved is the $2p \rightarrow (n-1)d$ instead of $1s \rightarrow np$. Secondly, the absorption takes place at much lower photon energies (for Mo, *ca.* 2500 eV at $L_{2,3}$-edges *vs.* 20 keV for the K-edge), so that an energy resolution of 0.5 eV or better can be achieved.[5,15] In addition, $L_{2,3}$-edges of molybdenum (2520 – 2625 eV) are close to the K-edges of light elements such as phosphorus (2140 eV), sulphur (2470 eV) or chlorine (2822 eV), so that these elements can be studied in a single measurement.

The apparent advantages of molybdenum $L_{2,3}$-edges come with practical difficulties. Measurements are done in the tender X-rays range, so that they need to be conducted in vacuum, which may be a challenging technical issue. When investigating the reactivity of Mo-based catalysts, *in situ* and *operando* experiments are performed, using environmental cells or other setups not compatible with transmission measurements or total electron yield collection. Fluorescence yield is then used as a versatile measurement mode, even though the fluorescence yield is not optimal when using tender x-rays.

In the present work, we show the spectra of a few selected compounds with diverse oxidation states, ligands and geometries and propose general guidelines for acquisition of XANES spectra at the Mo $L_{2,3}$-edges and their qualitative interpretation. Few of these compounds ($Na_2MoO_4$, $MoO_3$, $MoO_2$, $MoS_2$) were already studied in the literature using resonant inelastic X-ray scattering (RIXS) and FEFF modelling.[16] Although numerical calculations are a powerful tool to interpret such data, we focus here on a simple yet reliable method for a first interpretation, particularly intended for experimentalists performing measurements with no immediate access to such expertise (eg. during a synchrotron run). Besides, experimental data files of all the spectra are provided as supplementary materials, and made available to the community for comparison with theoretical models. Here, our approach is focused on fluorescence-detected XANES, a technique that is nowadays broadly available at synchrotrons, from a purely experimental perspective. We first briefly present the physics behind XAS at the $L_{2,3}$-edges applied to the case of molybdenum. Second, we discuss the impact of incident beam angle on self-absorption. Third, we present spectra of a few reference compounds, bundled according to their geometry. Fourth, we highlight the difficulties of measurements and discuss the impact of air exposure for sensitive compounds with exotic geometries. In particular, we report the $L_2$-edge and $L_3$-edge spectra of a series of

compounds, $(NH_4)_3Mo_{12}O_{40}P$, $Mo(OiPr)_5$, $[MoCp(CO)_3]_2$, $[Mo(acetate)_2]$, $(NH_4)_2[Mo_3S_{13}]$, $(NH_4)_2[Mo_3S_7Cl_6]$, which we discuss in relation with benchmark compounds such as $Na_2MoO_4$, $MoO_3$ and $(NH_4)_2MoS_4$. In the last part, we apply our guidelines to a series of molybdenum sulphide species, for which we propose an electronic structure. Both the data presented here and the interpretation guidelines that we propose should catalyse the use of XAS at the Mo $L_{2,3}$-edges as a unique tool to determine oxidation state and geometry in catalysts, thin films, composites, nanoparticles, molecular complexes, or metalloenzymes.

## 2. Experimental section

### 2.1 Mo-based compounds

$MoO_2(acac)_2$, $MoCl_3$ and $[MoCp(CO)_3]_2$ were purchased from Strem Chemicals and used as is. $MoO_2$, $MoO_3$, $MoCl_5$, $(NH_4)_6Mo_7O_{24}$, $Na_2MoO_4$, $Na_2MoO_4 \cdot 2H_2O$, $H_3Mo_{12}O_{40}P$ hydrate, $(NH_4)_3Mo_{12}O_{40}P$, $MoS_2$ and $(NH_4)_2MoS_4$ were purchased from Sigma-Aldrich and used as is. $Mo(OiPr)_5$ and $[Mo(acetate)_2]_2$ were purchased from Alfa-Aesar and used as is. $MoS_3$, amorphous $MoS_2$ (also referred to as "MoS$_2$ TD"), $(NH_4)_2[Mo_3Cl_{13}]$ and $(NH_4)_2[Mo_3S_7Cl_6]$ were synthesised according to reported procedures.[17–21] $Mo(acac)_3$ was synthesised according to a modified reported procedure.[22]

### 2.2 X-ray Absorption Spectroscopy

Sulfur K-edge and molybdenum $L_{2,3}$-edges XAS were performed on the LUCIA beamline at Synchrotron SOLEIL at an electron energy of 2.7 GeV and an average ring current of 450 mA with a Si(111) double crystal monochromator, with an energy resolution of 0.31 eV at 2500 eV and of 0.35 eV at 2700 eV. Data were collected in fluorescence mode with an SDD Bruker detector. The fluorescence detector formed an angle of 90° with the beam. The sample faced the beam, with an outgoing angle of 0.1° to 10° depending on the measurements.

For the compounds Mo(0), $MoO_2$, $MoO_3$, $(NH_4)_6Mo_7O_{24}$, $MoO_2(acac)_2$, $Mo(acac)_3$, $MoCl_3$, $MoCl_5$, $Na_2MoO_4$ and $Na_2MoO_4 \cdot 2H_2O$, data were recorded in flyscan mode between 2420 and 2750 eV, with an energy step of 0.2 eV and a 0.5 s time step. Data were recorded with energy steps of 0.2 eV at the edge and 1 eV elsewhere, with collection times of 3 s and 1 s, respectively.

4 to 6 mg of sample were diluted with *ca.* 40 mg of graphite (natural graphite powder, Ultra "F" purity >99.9%, from Alfa Aesar") and were compressed to form a 6 mm diameter pellet. Up to eight pellets were fixed with Kapton adhesive tape on a copper plate placed in a sample holder inside the chamber. During typical analyses, the pressure in the chamber was

maintained around $10^{-2}$ mbar. To measure air-sensitive compounds, we spread the compound directly on the carbon tape with a spatula in the glovebox. Then, we used a glass vessel filled with argon gas to bring the sample holder from the glovebox up to the beamline and flushed the pellet with a light flux of argon during the transfer into the analysis chamber. Each scan was repeated six times. For data reduction and treatment, we used Athena software to merge the different scans and eventually discard some of them. Pre-edge and post-edge backgrounds were subtracted from the XAS spectra and normalisation was done with respect to the $L_3$-edge. After normalisation, all spectra were smoothed using 11 repetitions of the three-point algorithm implemented in Athena software.

## 2.3 XAS of air-sensitive compounds

Air-sensitive compounds are difficult to analyse by XAS since presenting the sample in front of the beam usually exposes it to air. To circumvent this issue, we used a glass flask filled with argon gas to bring the sample holder with the compounds from a glovebox up to the beamline (see also experimental section), in order to maintain an inert atmosphere around the compound until the last moment and limit the oxidation to its minimum. A few grains of the sample were spread with a spatula, directly onto a piece of carbon tape attached to the sample holder and Kapton tape was used to seal the sample. Because the thickness of the sample is low in this configuration, we also measured the signal at the sulfur K-edge coming from sulfur inside the carbon tape (see spectrum of the bare carbon tape Figure S1). This contamination did not impact the signal measured at the Mo $L_{2,3}$-edges, as shown Figure S2. It should be noted that such strategy can easily be implemented at any beamline.

## 3. Results and discussion

## 3.1 Theory of XAS at the Mo $L_{2,3}$-edges

In X-ray absorption spectroscopy, core electrons are excited when absorbing an X-ray photon. Depending on the photon energy, a variety of physical processes occur, resulting in a variety of structures in the X-ray absorption spectrum. Here, we are interested in the XANES part of the spectrum (also known as NEXAFS), where the photon energy is around the transition energy (from a few eV below the absorption edge to *ca.* 50 eV above). After absorption of a photon, an electron is promoted from an occupied level to the first unoccupied levels, and then, for a higher energy, to the continuum, where it will interact through multiple scattering with the neighbouring atoms. This second, high energy region is known as the EXAFS (Extended X-ray Absorption Fine Structure) part. The analysis of the EXAFS part of

the spectra is out of scope of our work, so we will focus on analysing the XANES spectra of Mo-based compounds. The analysis of the XANES spectrum (peaks positions and intensities) provides qualitative information on the local symmetry around the atom and the electronic state, meaning in particular the oxidation and spin state. Because of the versatility of chemical environments and oxidation states of molybdenum, XANES at the $L_{2,3}$-edges is particularly informative to describe them.

XANES of 4d metals at the $L_{2,3}$-edges originates from the transition of electrons from a 2p orbital to a higher orbital, such as 4d orbitals (Figure 1). Due to spin-orbit coupling, the three 2p orbitals are divided in two groups: the $2p_{3/2}$ (2 orbitals – 4 electrons) and the $2p_{1/2}$ (1 orbital – 2 electrons), with the energy of the $2p_{3/2}$ orbitals being *ca.* 100 eV lower than the $2p_{1/2}$ orbitals for 4d transition metals.[23] As a consequence, the $L_3$-edge corresponds to the electronic transition $2p_{3/2}$ → 4d, while the $L_2$-edge (twice less probable so twice less intense) corresponds to the transition $2p_{1/2}$ → 4d. The $L_1$-edge technically exists and corresponds to the transition 2s → 4d. It provides the same information than the K-edge and is thus rarely studied.

An increase in oxidation state shifts the position of the XAS spectra towards higher energies because of the stabilisation of the 2p block. In other words, measuring the edge position is a convenient way to estimate the oxidation state of the element of interest. Measuring the edge position is easily done by taking the maximum of the first derivative of the spectra. Since the intensity is higher for the $L_3$-edge than for the $L_2$-edge, the position of the $L_3$-edge can be measured with a better accuracy.

If we now consider the five 4d orbitals, they are not all degenerated. According to crystal field theory, the symmetry around the metallic atom dictates how the 4d orbitals organise. In general, Mo adopts octahedral or tetrahedral geometries. In the case of an octahedron, the 4d orbitals will split in two groups, separated by a few eV: (i) three stabilised $t_{2g}$ orbitals and (ii) two destabilised $e_g$ orbitals. For a tetrahedron, a splitting is also expected, except that the e orbitals are now stabilised and thus lower in energy than the $t_2$ orbitals. The corresponding $L_2$ and $L_3$ XANES spectra are thus expected to be doublets, with an intensity ratio of 3:2 for octahedral geometries and of 2:3 for tetrahedral geometries, so the shape of the spectrum gives a first indication on the geometry around Mo.
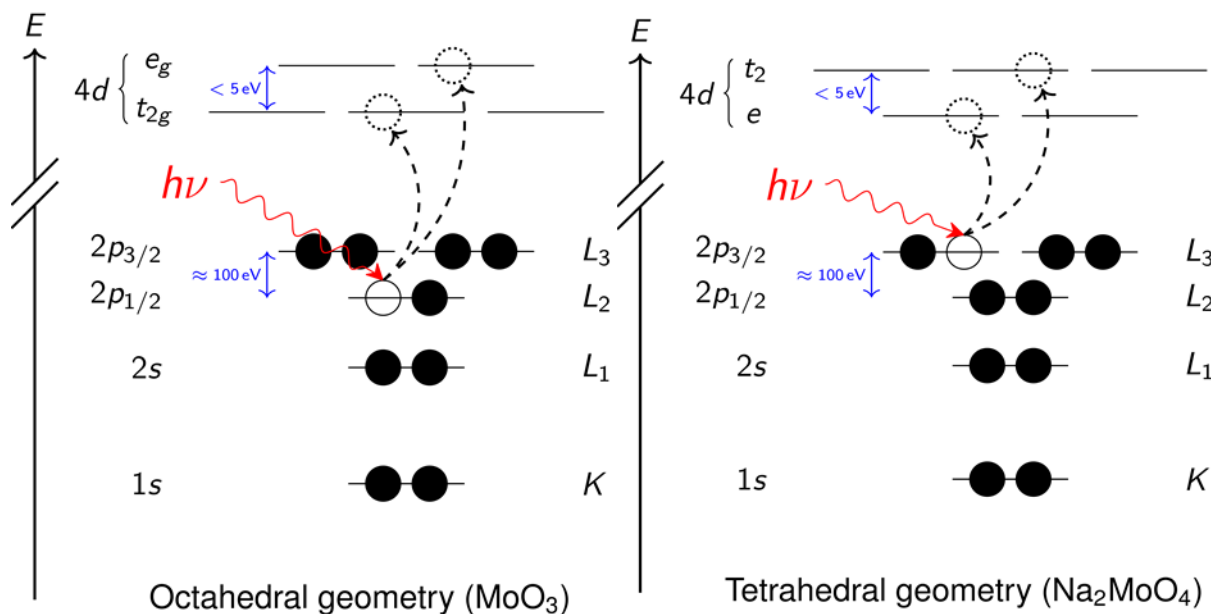
**Figure 1** – Schematic diagram of the atomic orbitals involved in XANES at the $L_2$- (left) and $L_3$-edges (right) for a 4d transition metal in octahedral (left) or tetrahedral geometry (right).

The geometry around Mo can be deduced in a more accurate way. In the framework of crystal field theory, the splitting $\Delta$ of the d orbitals is admittedly higher in octahedral geometry (6 ligands) $\Delta_o$ than in tetrahedral geometry $\Delta_t$ (4 ligands). In practice, the 4d-splittings measured for Mo in octahedral environments are superior than splittings observed for Mo in tetrahedral environments: in the literature, compounds for which Mo is in an octahedral environment – such as $MoO_3$ – present splittings at both the $L_3$ and $L_2$ edges ranging between 2.8 and 4.5 eV.[4,5,24] For tetrahedral compounds – such as $Na_2MoO_4$ – the splittings range between 1.8 and 2.6 eV at both the $L_3$ and $L_2$ edges.[4,5,24,25] In other words, measuring the splittings in $L_{2,3}$-edges is a reliable way to determine the geometry around Mo atoms.

Besides the crystal field considerations presented above, the geometry analysis is impacted by the presence of multiplet effects. These effects include mostly spin-orbit coupling and correlations between the orbital of departure (here 2p) and of arrival of the electron (here 4p). Multiplet effect were previously estimated using explicit Hartree-Fock computations and are known to alter the shape of the spectra at the $L_{2,3}$-edges, by impacting the $L_3/L_2$ intensity ratio.[23,26–28] An exhaustive description is beyond the scope of the present paper, but two major consequences of the multiplet effects arise from theoretical considerations. First, the impact of the multiplet effects on the $L_3/L_2$ ratio depends on the number of electrons in the 4d orbitals. In other words, the shape of the $L_{2,3}$-edges is directly impacted by the oxidation state. Building a collection of experimental spectra from reference compounds at different oxidation states is thus a timely endeavour.[23,27] Second, for 4d

8

transition metals, the multiplet effects are expected to be less important for the $L_2$-edge than for the $L_3$-edge since the $2p_{3/2}$ orbitals have a smaller overlap than the $2p_{1/2}$ orbitals with the final 4d orbitals.[23] It is thus more rigorous to use the $L_2$-edge to determine the symmetry of Mo. In practice, because the splittings are small ($< 5$ eV) compared to the edge position (2500 eV for Mo $L_{2,3}$-edges), they are difficult to resolve directly on the spectra. The splitting of the 4d orbitals can be more easily determined on the second derivative spectra, as the spacing between the two negative contributions.

Altogether, we propose using the first derivative of the spectra, preferably at the $L_3$-edge, to determine the oxidation state of Mo and using the second derivative of the spectra, preferably at the $L_2$-edge, to gain insight on the geometry around molybdenum. In the section below, we validate this methodology by examining first the spectra of a few reference compounds. In particular, we easily retrieve evidences of their expected structure. Therefore, the following discussion is organised based on the geometry around Mo.

### 3.2 Overcoming the Limitations of Fluorescence Recording Mode

As a starting point and validation of our measurements, we present the spectrum of bulk metallic molybdenum on Figure 2. We polished a block of bulk metallic molybdenum for a few minutes before measuring its fluorescence XANES spectrum. The edges positions are evaluated as the positions of the two maxima of the derivative. We find that the $L_3$-edge is located at 2520.4 eV and the $L_2$-edge is at 2625.3 eV. Considering an energy resolution of *ca.* 0.5 eV[15], these values are consistent with the values of the binding energies of the $2p_{3/2}$ and $2p_{1/2}$ orbitals of Mo (2520.2 and 2625.1 eV, respectively) evaluated by Bearden *et al.* and used as standards in the ubiquitous X-ray booklet.[29]
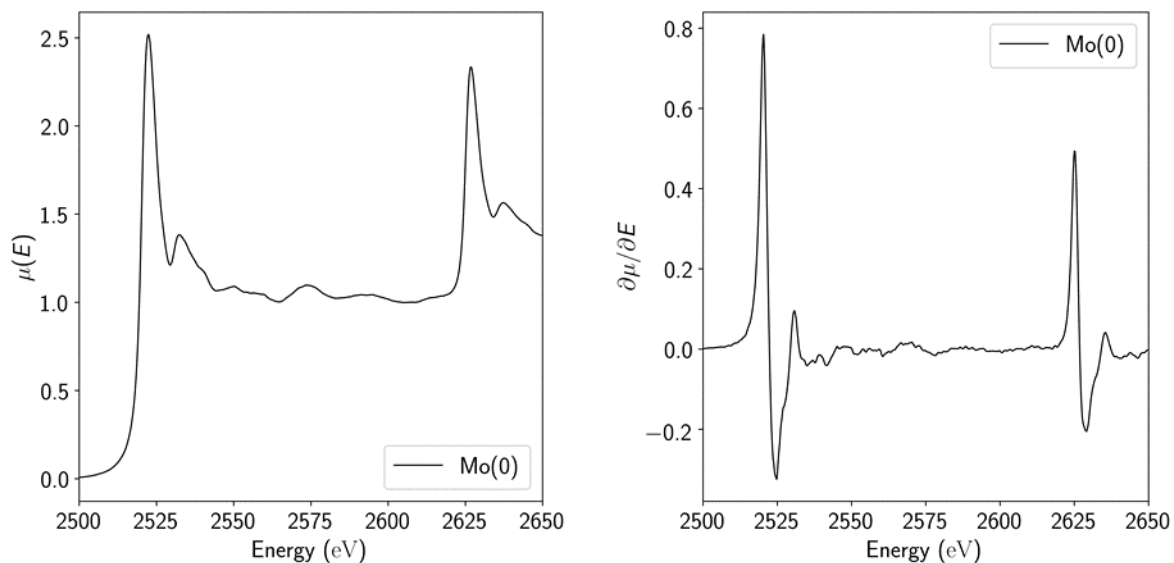
Ideally, XAS measurements are performed in transmission mode. However, in the tender X-ray range, absorption by the sample is strong and this mode is much harder to implement than a measurement using the total electron yield or partial fluorescence yield. Moreover, *in situ* and *operando* setups are much easier to perform in fluorescence than in transmission mode. In this regard, collecting fluorescence mode reference spectra is more rigorous if these data are to be compared with other ones collected in fluorescence mode with *in situ* and *operando* setups. This is the reason why all the XAS presented in this work were done using Partial Fluorescence Yield. The main limitation in this mode is self-absorption of the emitted X-rays in the sample. In this section, we discuss how to overcome this on the practical case of Mo L$_{2,3}$-edges measurement.

The best way to prevent self-absorption is to dilute the sample. However, dilution is done at the expense of signal-to-noise ratio. A way to circumvent this issue is to decrease the beam incident angle so that only the signal of fluorescence coming from surface atoms, where self-absorption is less likely, is detected. Here, we illustrate this strategy on XANES of commercial MoS$_2$. We prepared compressed pellets containing 1w% or 10w% and recorded XANES spectra with the two concentrations. In the case of the 1w% pellet, we tested two different incident beam angles, 2° and 10°. The three XAS spectra (1% 2°, 1% 10° and 10% 2°) are shown on Figure 3 and evidence an increase in the L$_3$/L$_2$ ratio when the concentration in Mo or the incident beam angle is increased, due to self-absorption. To further evidence how critical the recording conditions are, we also show on Figure 3 the XANES spectra of Mo(acac)$_3$ (10w%) with incident beam angles of 5° and 0.1°. As evidenced on

Figure 3, self-absorption occurs when the incident beam angle is 5°, causing the $L_3/L_2$ intensity ratio to decrease and deviate strongly from 2. By decreasing the angle to 0.1°, we thus decreased the occurrence of self-absorption and retrieved a $L_3/L_2$ ratio of 2, indicating the spectra are less afflicted by self-absorption. Self-absorption depends also on the nature of the compound, so it is not possible to establish universally-valid optimised recording conditions. Instead, a compromise between occurrence of self-absorption and signal-to-noise ratio has to be found by playing on the concentration and the incident beam angle.
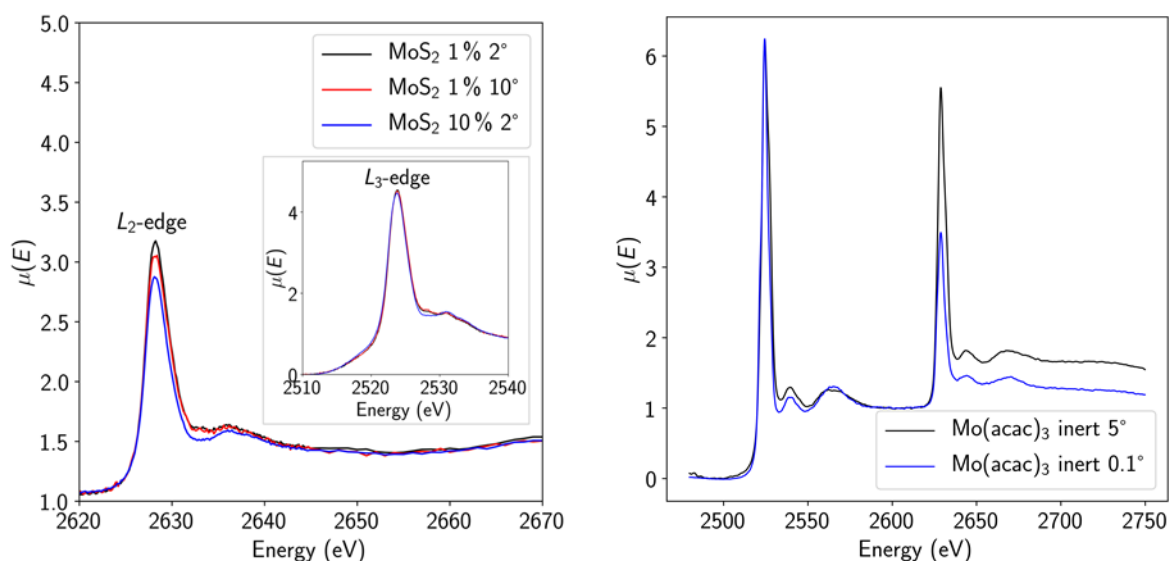


**Figure 3 – Left: XANES spectra of commercial MoS₂ measured at different concentrations and incident beam angles. For an easier comparison, the spectra were normalized *vs.* the intensity of the L₃-edge. Right: XANES data of Mo(acac)₃ recorded with 5° (black) and 0.1° (blue) incident beam angle.**

## 3.3 Geometric analysis

### 3.3.1 Inorganic compounds in Oh geometry

According to their crystal structures, inorganic compounds with Mo in an octahedral, or distorted octahedral, geometry include: $MoO_2$, $MoO_3$, $(NH_4)_6Mo_7O_{24}$, the acid/base couple $H_3Mo_{12}O_{40}P/(NH_4)_3Mo_{12}O_{40}P$, $MoO_2(acac)_2$, $Mo(acac)_3$, $MoCl_3$ and $MoCl_5$, with acac⁻ being the acetylacetonate anion, $C_5H_8O^-$. These octahedral compounds together provide formal oxidation states from (+III) to (+VI) and cover different type of compounds: bulk materials, coordination complexes and polyoxometalate anions. Their crystal structures are presented on Figure 4.

Some of Mo compounds, such as $MoO_3$ and $Na_2MoO_4$ and $(NH_4)_2MoS_4$ are often used as references in works discussing new Mo compounds.[4,13] These are especially useful to

benchmark spectroscopic data across time, or coming from a variety of experimental setups. Besides, the L$_3$-edges were reported for H$_3$Mo$_{12}$O$_{40}$P and MoO$_2$(acac)$_2$ but not the L$_2$-edge was measured.[30]
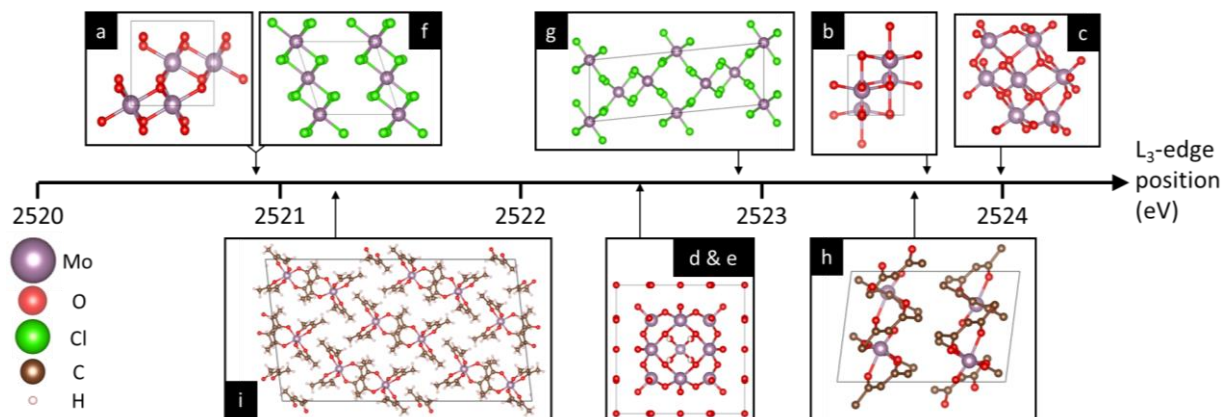


**Figure 4 – Crystal structures and positions of the L$_3$-edges of the Mo-based octahedral compounds studied in this work. a) MoO$_2$, b) MoO$_3$, c) (NH$_4$)$_2$Mo$_7$O$_{24}$, d) & e) [Mo$_{12}$O$_{40}$P]$^{3-}$ anion (half occupancy oxygen atoms are displayed as red and white spheres), f) MoCl$_3$, g) MoCl$_5$, h) MoO$_2$(acac)$_2$, i) Mo(acac)$_3$. Extracted from refs [31, 32, 33,34, 35, 36, 37, 38, 39] and [40] respectively.**

We diluted all nine compounds in graphite and put them under the form of pellets (MoCl$_3$ and MoCl$_5$ are moisture and air sensitive, so we maintained an inert atmosphere above their pellets, see details in experimental section). The XAS spectra of these nine compounds were measured at the Mo L$_{2,3}$-edges. The data (spectra, second derivative and first derivative) are presented on Figure 5.
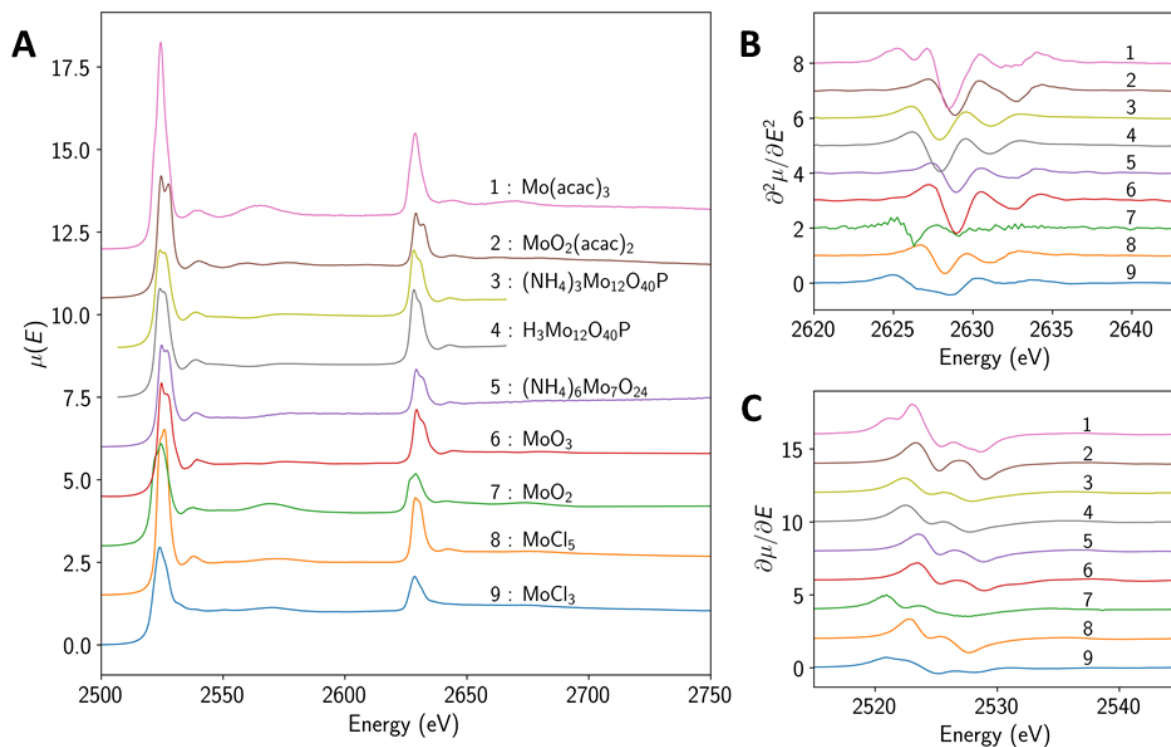
**Figure 5 - XANES data at the L$_{2,3}$-edges of octahedral Mo compounds. A: XANES spectra, B: XANES second derivative at the L$_2$-edge, and C: XANES first derivative at the L$_3$-edge.**

As expected, the overall shapes of the spectra are similar, with absorption edges exhibiting doublets due to crystal field splitting. The best estimations of the splittings were made using the second derivatives of the spectra at the L$_2$-edge. We found splittings between 2.9 and 3.9 eV, in good agreement with the expected splittings for octahedral Mo compounds ranging from 2.8 to 4.5 eV.[4,5,23,24] Overall, the splittings are greater for compounds with oxygen than for compounds with chlorine, which is expected from the spectrochemical series: the ligand strength of oxygen-based ligands (O$^{2-}$, acac$^-$) is higher than the strength of Cl$^-$ ligands.

Then, we measured the position of the maximum of the first derivative at the L$_3$-edge. In these compounds, we obtain average L$_3$-edge positions of 2521.1, 2520.9, 2522.9 and 2523.2 eV for Mo(+III), Mo(+IV), Mo(+V) and Mo(+VI) formal oxidation states, respectively (see Table 1). We notice that for (+III) and (+IV) redox states, the L$_3$-edge position is around 2521 eV, while for (+V) and (+VI) redox states, the L$_3$-edge position is around 2523 eV. These results are displayed on Figure 6. As expected, the position of the L$_3$-edge depends on the oxidation state, so that no compounds with a low oxidation state (*i.e.,* lower than or equal to (+IV)) have their L$_3$-edge below 2521.5 eV. For (+V) oxidation states, the L$_3$-edge is increased abruptly to *ca.* 2523 eV. For the (+VI) oxidation states, compounds where Mo is only linked to oxygen atoms have their L$_3$-edge at 2523.5 eV or above, up to 2524.0 eV. However, Mo(+VI) compounds containing sulfur and phosphorous have an L$_3$-

edge between 2522.4 and 2522.5 eV. This difference of 1.1 to 1.6 eV is due to the low electronegativity of the P and S atoms, compared to oxygen. Overall, the link between oxidation state and position of the $L_3$-edge appears to be neither linear nor monotonous, so that one can only infer an approximated value of the oxidation state from a XAS measurement at the $L_{2,3}$-edges.

| Compound (formal redox state) | Position of the $L_3$-edge (eV) | Position of the $L_2$-edge (eV) | Splitting at the $L_3$-edge (eV) | Splitting at the $L_2$-edge (eV) |
|---|---|---|---|---|
| Mo(acac)$_3$ (+III) | 2521.2 | 2627.7 | 3.6 | 3.8 |
| MoO$_2$(acac)$_2$ (+VI) | 2523.6 | 2628.1 | 3.8 | 3.9 |
| (NH$_4$)$_3$Mo$_{12}$O$_{40}$P (+VI) | 2522.5 | 2626.9 | 3.3 | 3.4 |
| H$_3$Mo$_{12}$O$_{40}$P (+VI) | 2522.4 | 2627.0 | 2.9 | 3.1 |
| (NH$_4$)$_6$Mo$_7$O$_{24}$ (+VI) | 2524.0 | 2628.2 | 3.6 | 3.3 |
| MoO$_3$ (+VI) | 2523.7 | 2628.1 | 3.8 | 3.5 |
| MoO$_2$ (+IV) | 2520.9 | 2625.9 | 2.9 | 2.8 |
| MoCl$_5$ (+V) | 2522.9 | 2627.6 | 3.2 | 2.9 |
| MoCl$_3$ (+III) | 2520.9 | 2626.0 | 3.6 | 3.4 |

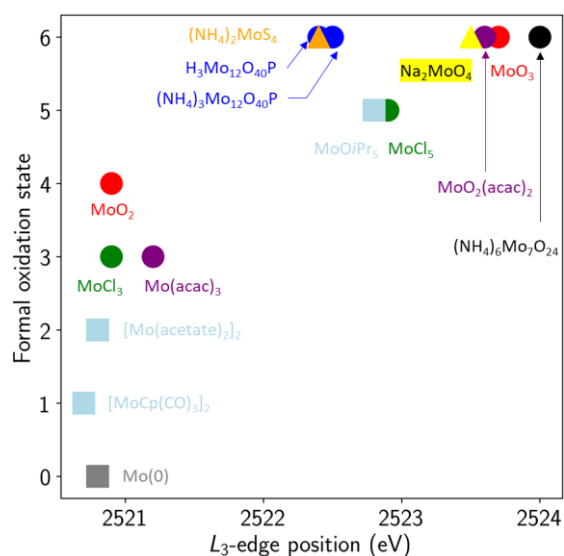Table 1 - Extracted parameters for octahedral inorganic compounds.



Figure 6 – Formal oxidation state as a function of the $L_3$-edge position. Circles show the compounds in octahedral geometry, triangles are for tetrahedral compounds and squares are for other geometries.

### 3.3.2 Inorganic compounds in Td geometry

The molybdate anion MoO$_4^{2-}$ is an ubiquitous building block of polymetallic structures containing Mo(+VI). Except for salts containing the MoO$_4^{2-}$ anion and its sulfurised analogue MoS$_4^{2-}$, there are few common inorganic compounds with Mo in a tetrahedral geometry available. We thus measured XAS at Mo $L_{2,3}$-edges of pellets made of anhydrous

$Na_2MoO_4$, $Na_2MoO_4 \cdot 2\ H_2O$ and $(NH_4)_2MoS_4$. The spectra, the second and the first derivative are shown on Figure 7. Anhydrous and di-hydrated sodium molybdate exhibit very similar spectra (see also Table 2). For both compounds, the maximum of the first derivative of the $L_3$-edge is located at 2523.5 eV, in good agreement with the position of Mo(+VI) oxides in octahedral geometry (see Table 1 and Figure 6).[5,25] Their splitting at the $L_2$-edge is of 2.2 eV, in good agreement with the expected splitting of 1.8 to 2.6 eV for tetrahedral species.[5] Regarding ammonium tetrathiomolybdate, for which Mo is formally at the (+VI) oxidation state, the maximum of the first derivative at the $L_3$-edge is located at 2522.4 eV. This value is 1 eV lower than these of Mo(+VI) compounds, but is also 1.5 eV higher than the value of 2520.9 eV measured for $MoO_2$ (oxidation state of +IV). This intermediate position can be attributed to $S^{2-}$ ligands, which may give additional electronic density from their non-bonding orbitals. From the spectrochemical series, the sulfide ligands are weaker field ligands than $O^{2-}$. Consistently, the splitting measured at the $L_2$-edge is of 1.0 eV (*vs.* 2.2 eV for molybdate), confirming the crystal field splitting from the sulfide ligands is much weaker than the splitting from oxo ligands.
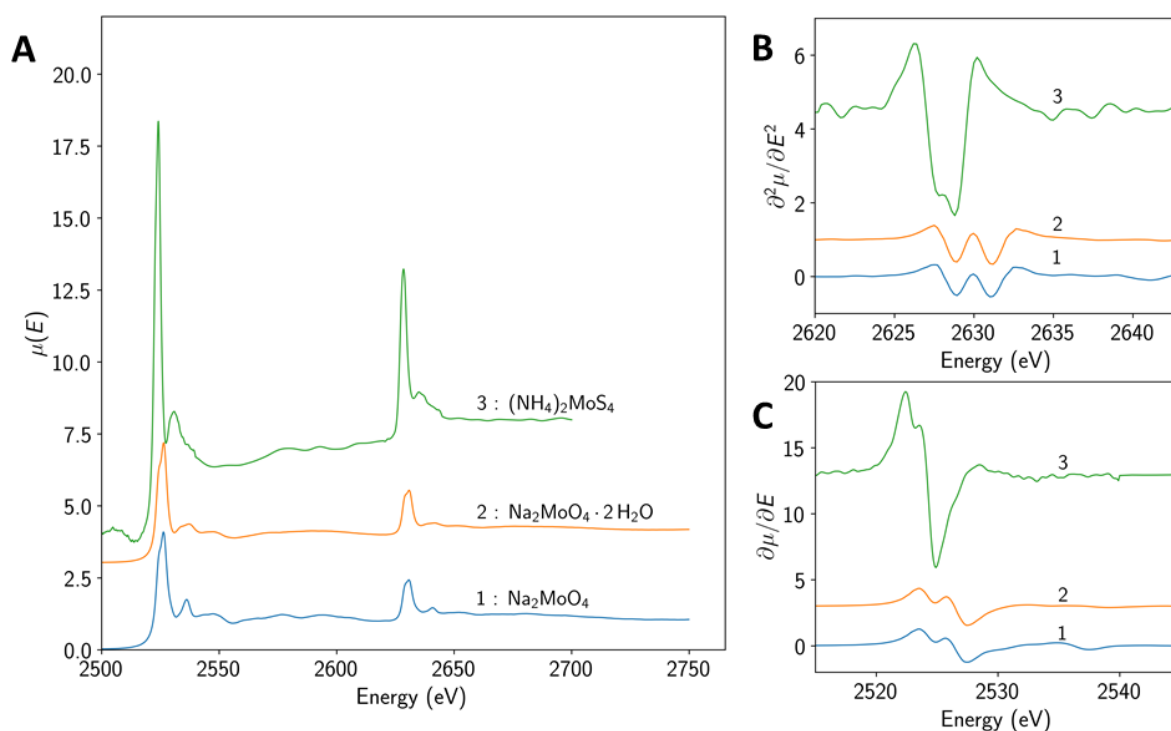


Figure 7 - XANES data at the $L_{2,3}$-edges of tetrahedral Mo compounds. A: XANES spectra, B: XANES second derivative at the $L_2$-edge, and C: XANES first derivative at the $L_3$-edge.

| Compound (formal redox state) | Position of the $L_3$-edge (eV) | Position of the $L_2$-edge (eV) | Splitting at the $L_3$-edge (eV) | Splitting at the $L_2$-edge (eV) |
|---|---|---|---|---|
| $(NH_4)_2MoS_4$ (+VI) | 2522.4 | 2627.0 | 1.5 | 1.0 |
| $Na_2MoO_4 \cdot 2H_2O$ (+VI) | 2523.5 | 2628.2 | 2.4 | 2.2 |
| $Na_2MoO_4$ (+VI) | 2523.5 | 2628.2 | 2.4 | 2.2 |

**Table 2 - Extracted parameters for tetrahedral inorganic compounds.**

As stated in the subsection regarding the theory of XAS at the $L_{2,3}$-edges, the shape of the spectra depend on the geometry: the intensity ratios at both the $L_3$-edge and the $L_2$-edge are expected to be 3:2 and 2:3 for an octahedral and a tetrahedral geometry, respectively. Accordingly, our spectra for octahedral compounds have a first contribution that is more intense than the second one, while it is the opposite for tetrahedral compounds. To discriminate more rigorously the geometry, we showed that large splittings are linked to compounds in octahedral geometries, whereas smaller splittings are the signature of tetrahedral compounds. At this point, we presented data limited to either octahedral or tetrahedral compounds, with an oxidation state above (+III). Other geometries and lower oxidations states exist and we present some compounds fitting one or both criteria in the next section.

### 3.3.3 Accessing low oxidation states and exotic geometries with air-sensitive compounds

In the previous sections, we only showed examples where Mo is in an oxidation state higher or equal to (+III), with either octahedral or tetrahedral geometries. However, in the case of *operando* experiments using Mo species as a catalyst, intermediate species with a lower oxidation state than (+III) and a geometry different than octahedral or tetrahedral could be involved. These intermediates can hardly be isolated, therefore having available reference spectra of compounds containing Mo in low oxidation state and in exotic geometries is of particular interest.

We measured the XAS signal of pellets of three air-sensitive, less studied Mo-based organometallic compounds (Figure 8): $Mo(OiPr)_5$, $[MoCp(CO)_3]_2$ and $[Mo(acetate)_2]_2$ where $i$Pr is the isopropyl (or 1-methylethyl) group, $Cp^-$ is the cyclopentadienyl anion $C_5H_5^-$ and acetate is the $CH_3CO_2^-$ anion. In $Mo(OiPr)_5$, Mo is expected to be in the (+V) oxidation state, in the dimer $[MoCp(CO)_3]_2$, Mo is expected to be (+I) and in the dimer $[Mo(acetate)_2]_2$, Mo is expected to be (+II). We later recorded again the signal of these compounds after a few hours

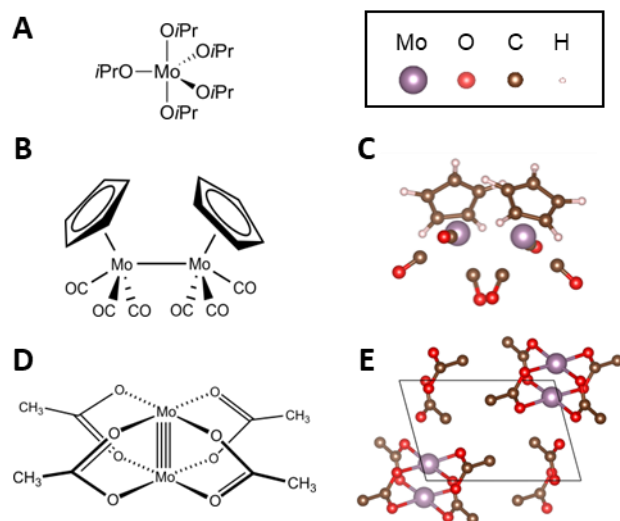of exposure to air to evidence the relevance of measurements performed under "inert" conditions.



**Figure 8 - Air-sensitive compounds studied in this work. A : representation of Mo(OiPr)$_5$ based on our proposed bipyramidal trigonal geometry, B & C, resp. : representation of [MoCp(CO)$_3$]$_2$ dimer and its crystal structure from Gould et al.[41], D & E, resp. : representation of [Mo(acetate)$_2$]$_2$ dimer and its crystal structure from Cotton et al.[42]**

To the best of our knowledge, the structure of Mo(OiPr)$_5$ has not been determined by monocrystal X-ray diffraction. Mo(OiPr)$_5$ is a compound very close to molybdenum *tert*-butoxide since in Mo(OtBu)$_5$ (tBu = *tert*-butyl or 1,1-dimethylethyl group), except for the number and arrangement of carbon atoms in the alkyl chain of their ligands. The synthesis of Mo(OtBu)$_5$ has been reported in April 2020 as the first homoleptic, all-oxygen-ligated but non-oxo 4d$^1$ Mo(V) complex.[43] Its structure was reported as an unperfect trigonal bipyramid. Based on the proximity with Mo(OtBu)$_5$, we propose that the native geometry of Mo(OiPr)$_5$ is also trigonal bipyramidal, but too unstable to be observed under air. When protected from air, the first derivative of the L$_3$-edge XANES spectrum (Figure 9) of Mo(OiPr)$_5$ has its maximum located at 2522.8 eV, confirming that Mo is in a high oxidation state. An additional, sharp feature can also be observed at 2536 eV at the L$_3$-edge and at 2640 eV at the L$_2$-edge, *ca.* 10 eV above the absorption edges. It is also present in the second derivative of the spectrum. This feature correlates well with the theoretical geometry of a 5-fold coordinated metal in trigonal bipyramidal geometry. Indeed, for Mo in this environment, we expect the splitting of the 4d orbitals to be as follows: $d_{xz} = d_{yz} < d_{xy} = d_{x^2-y^2} \ll d_{z^2}$. In other words, we expect three features, two of them close in energy and the third at a much higher energy. This description corresponds exactly to what we observed, particularly from the second derivative of the spectrum: the first two features are separated by a splitting of 2.15 eV, and the third

minimum is located 9.90 eV higher in energy than the second minimum. Upon air exposure, the third, high energy feature attributed to the 2p $\rightarrow$ 4d$_{z^2}$ transition partly disappears, which is consistent with the fact that the Mo(O*i*Pr)$_5$ compound is probably unstable (no structural characterisation in the literature). We thus have evidence of the degradation of molybdenum isopropoxide under exposition to air and propose that molybdenum isopropoxide does have a bipyramidal trigonal structure as long as it is protected from air.
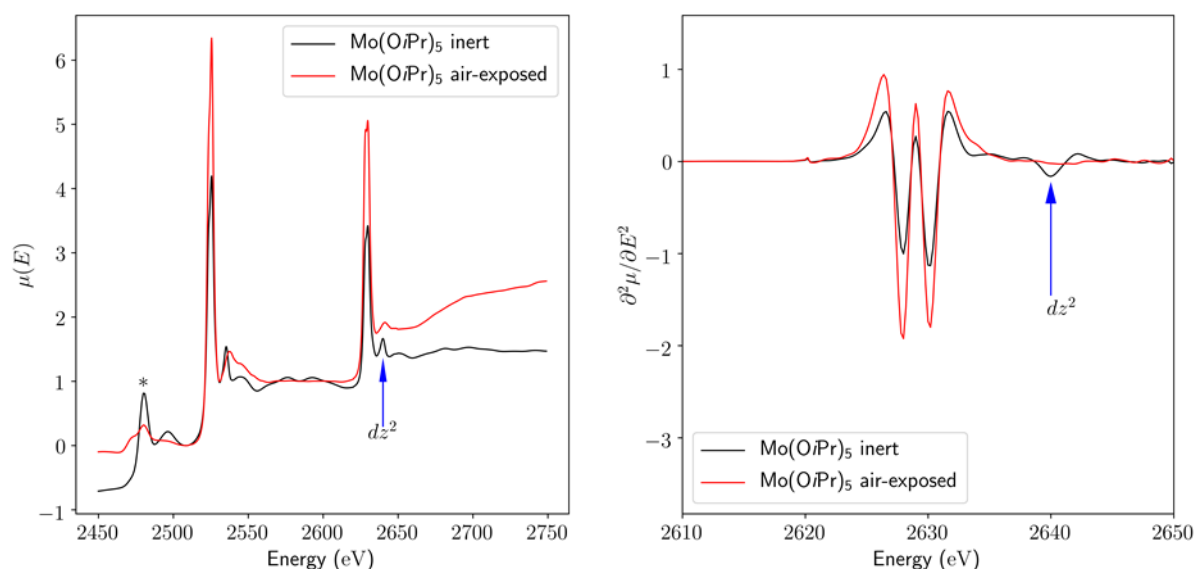


**Figure 9 - XANES data and second derivative of Mo(O*i*Pr)$_5$ recorded first in inert conditions then after ageing in air. The asterisk points out a contamination of sulfur from the carbon tape.**

In [MoCp(CO)$_3$]$_2$, Mo has a formal redox state of (+I) (see Figure 10). Accordingly, the maximum of the derivative of the L$_3$-edge is located at 2520.7 eV. At the L$_2$-edge, we do not notice any splitting (Figure 10). This observation is not consistent with the reported octahedral geometry[41] but instead is consistent with a low-spin tetrahedral geometry: in a (+I) redox state, Mo has 5 electrons in the 4d orbitals, so in a tetrahedral geometry with strong field ligands such as CO, the e orbitals are filled and there is only one transition possible to the t$_2$ orbitals. This disagreement could be linked to the long Mo-Mo distance in the dimer (3.22Å), leading to a very low orbital overlap between the two metals. Also, XANES probes the unoccupied states, so if the unoccupied states of the dimer do not involve a strong overlap between the orbitals of the two molybdenum atoms, it is possible that the second Mo atom is invisible by XANES. For this compound, not much effect of the air exposition is noticed (see Figure S3).
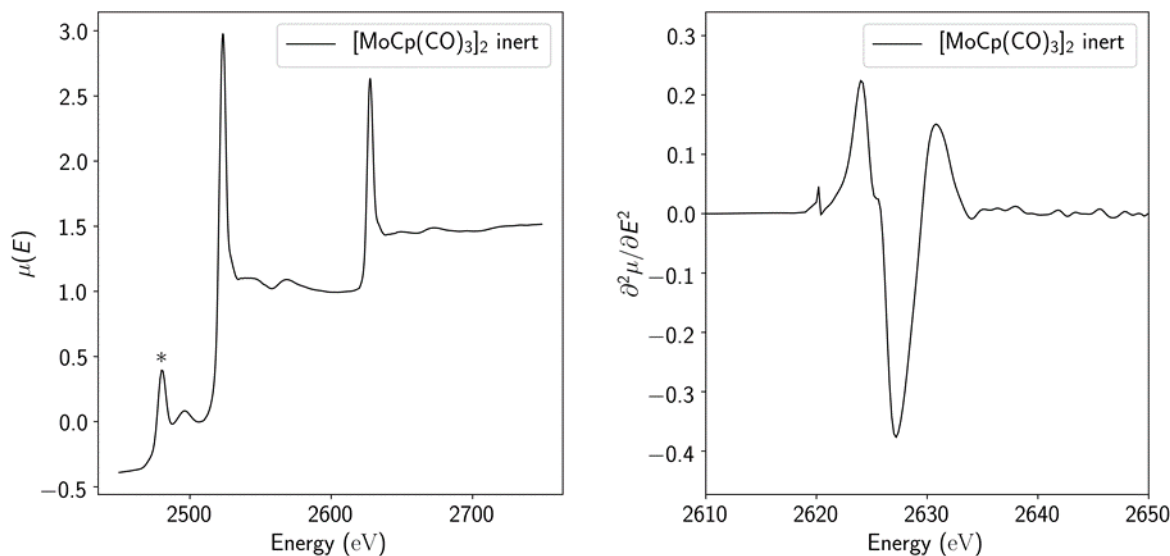
**Figure 10 - XANES data and second derivative of [CpMo(CO)₃]₂ recorded in inert conditions. The asterisk points out a contamination of sulfur from the carbon tape.**

In [Mo(acetate)₂]₂, Mo has a formal redox state of (+II) (see Figure 11). The maximum of the first derivative of the spectrum is at 2520.8 eV, corresponding to Mo in a lower oxidation state. The molybdenum acetate dimer adopts a "carboxylate-bridged" structure, identical to other metallic acetate dimers.[44] Each acetate ligand is linked to both metallic centres by its two oxygen atoms and the average Mo-O distance is 2.10 Å. The four oxygen atoms attached to a Mo centre form a slightly distorted square-planar configuration. In addition, the two Mo atoms are connected via a quadruple bond 2.11 Å long.[42,45] This Mo-Mo distance is almost equal to the Mo-O distance, so in this case the Mo-Mo bond must probably be taken into account for a geometrical description. From this description, the geometry around Mo is square pyramidal, so the splitting of the 4d orbitals is expected to be: $d_{xz} = d_{yz} < d_{xy} < d_{z^2} < d_{x^2-y^2}$. We thus expect up to four transitions on the second derivative of the XANES spectrum. These four transitions are seen Figure 11, on the second derivative of the XANES spectrum at Mo L₂,₃-edges under inert conditions. At the L₂-edge, they are located at 2626.5, 2628.1, 2632.1 and 2636.1 eV, leading to three consecutive splittings, of 1.6, 4.0 and 4.0 eV respectively. Exposing molybdenum acetate to air results in drastic changes in the shape of the spectrum: the maxima at 2532.1 and 2636.1 eV disappear. Similarly, the shape of the second derivative is altered, with the disappearance of the minima at 2626.8 and 2632.1 eV and the appearance of a new minimum at 2630.6 eV.
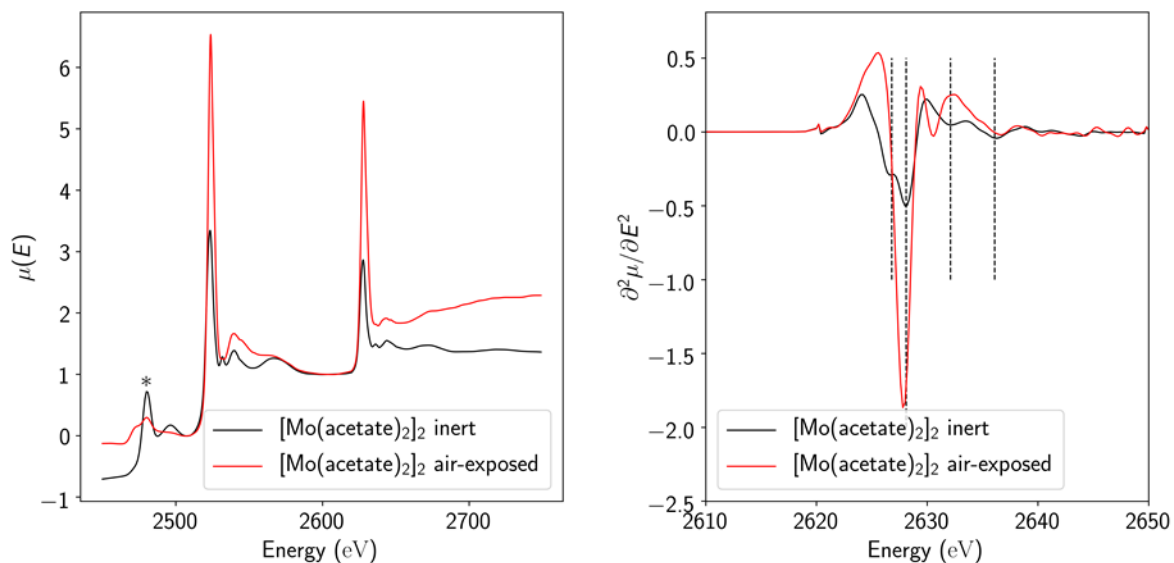
19

**Figure 11 - XANES spectrum (left) and second derivative (right) of [Mo(acetate)$_2$]$_2$ dimer, measured in inert conditions and after exposure to air. The asterisk points out a contamination of S from the carbon tape.**

In this section, by measuring air-sensitive compounds, we measured the XAS data of compounds where Mo is in an oxidation state lower than (+III) and in exotic geometries. We demonstrated that analysis of the second derivative of the XANES spectra at the Mo L$_{2,3}$-edges allows to determine the geometry around the Mo atoms. As far as oxidation states are concerned, the analysis is more complex for such complexes, since delocalisation and back-donation effects may invalidate the too simplistic crystal-field based analysis. It should be noted that, although this is out of the scope of the present work, complementary measurements at the Mo K-edge, which can be analysed with multivariate component analysis methods for instance, may be of interest for further analysis of the compounds.[46]

## 3.4 Application of XANES at the Mo L$_{2,3}$ edges to the family of molybdenum sulfides

Here, we aim using XANES at the Mo L$_{2,3}$-edges to describe the environment around Mo atoms of a few molybdenum sulfide compounds (Mo$_x$S$_y$). Spectra of a variety of molybdenum sulfide compounds are available in the literature, eg. MoS$_2$ and MoS$_3$ prepared by electrodeposition,[47] and, depending on the preparation route, they may be non-stoichiometric, defective or partly amorphous. Here, powders are measured, some of them commercial, the others prepared accorded to reported procedures (see experimental section). As a starting point, we measure (Figure 12) a commercial powder (average grain size: 90 nm) of the ubiquitous MoS$_2$ compound, crystallised in the hexagonal phase (2H). From the density

of states of 2H-MoS$_2$,[48] the lowest unoccupied states contain mostly contributions of the 4d orbitals. They are not very well separated and instead form a continuous feature of width equal to *ca.* 2.5 eV. Accordingly, the second derivative of the XANES spectrum shows a single feature. More precisely, on the second derivative of the XANES spectrum, we note a single feature with a width of roughly 2.2 eV (see Figure 12).
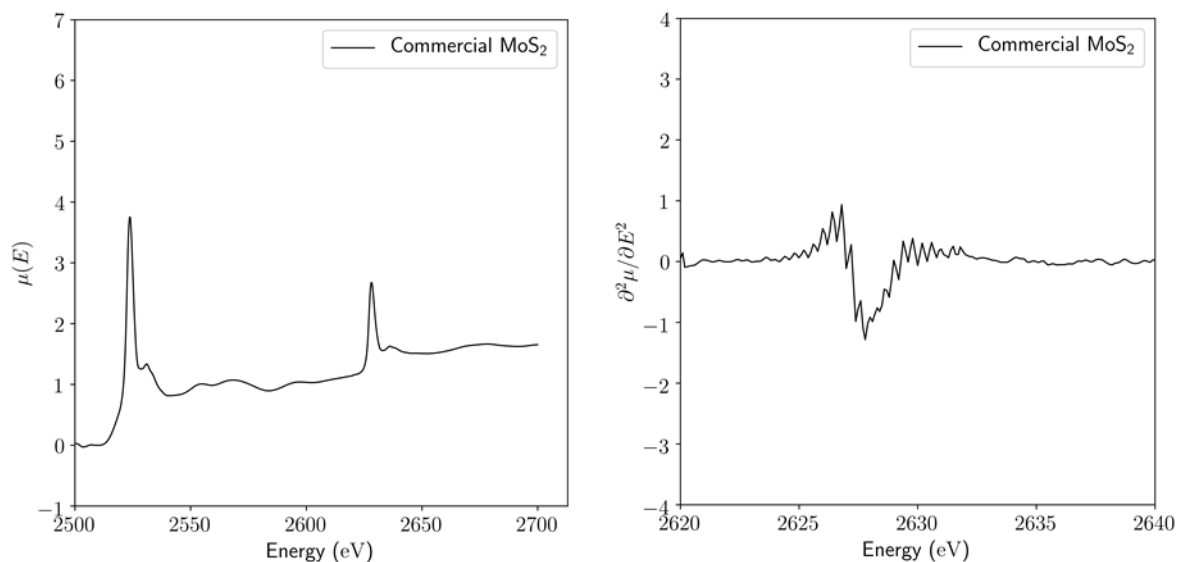


Figure 12 - XANES of Mo at L$_{2,3}$-edges (left) and second derivative at the L$_2$-edge (right) of commercial MoS$_2$.

Molybdenum sulfide phases (MoS$_x$) are active catalysts for the Hydrodesulfurisation (HDS) reaction[1,2] and Hydrogen Evolution Reaction (HER).[17,49–51] They can be produced by a two-step thermal decomposition under inert atmosphere: in a first step, (NH$_4$)$_2$MoS$_4$ decomposes to MoS$_3$ at 260 °C[17], releasing ammonia (NH$_3$) and hydrogen sulfide (H$_2$S). Then, heating up to 400 °C leads to the formation of amorphous MoS$_2$.[18]

$$(NH_4)_2MoS_4 \xrightarrow{\Delta\ 260\ °C} MoS_3 + 2\ NH_3 + H_2S$$

$$MoS_3 \xrightarrow{\Delta\ 400\ °C} MoS_2 + S$$
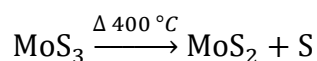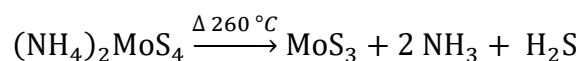
Following these protocols, we produced MoS$_3$ and amorphous MoS$_2$ (referred to as MoS$_2$ TD in the following), and measured their XANES signal at the Mo L$_{2,3}$-edges and S K-edge (Figure 13 and Figure 14). For the three compounds, commercial MoS$_2$, MoS$_2$ TD and MoS$_3$, the spectra are highly similar. The Mo L$_3$-edge and L$_2$-edge are located *ca.* 2522.5 and 2627.1 eV in all three cases (see Table 3), and the second derivatives of the spectra all exhibit a single feature *ca.* 2.2 eV large. Regarding the S K-edge, the edge position is expected between 2470 and 2475 eV for reduced sulfur species.[52] Here, we estimate the edge position

at 2470.1 eV for both commercial $MoS_2$ and $MoS_2$ TD, and 2470.3 eV for $MoS_3$. These values remain very close (see also Table 3), confirming that sulfur atoms are in close environments in all three samples.
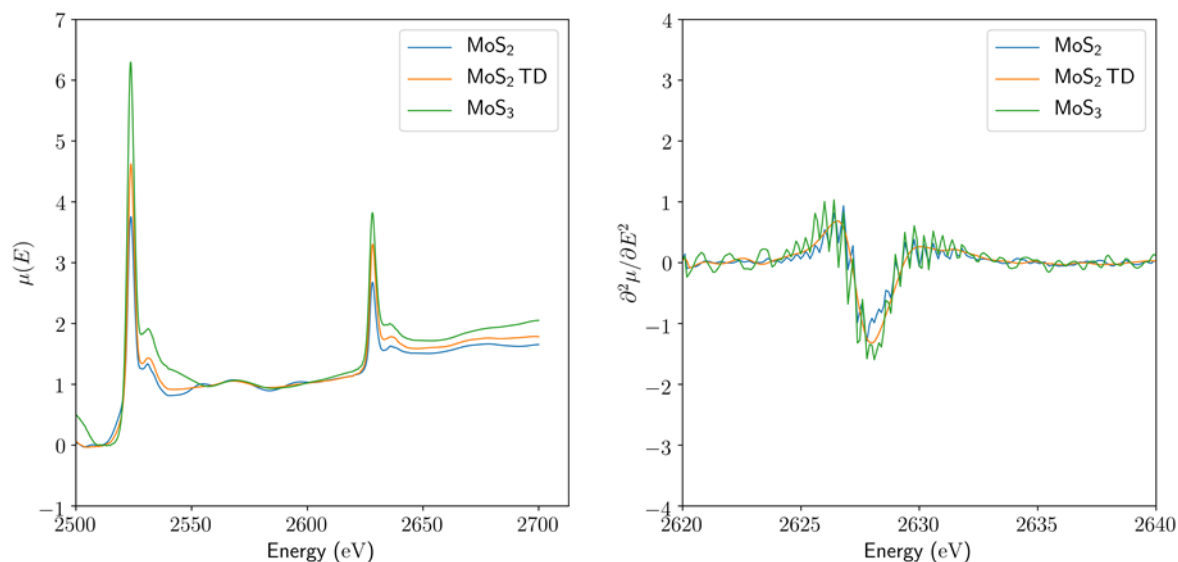


**Figure 13 – Left: XANES of commercial MoS₂, MoS₂ TD and MoS₃ compounds at Mo L₂,₃-edges. Right: second derivative of the L₂-edge.**
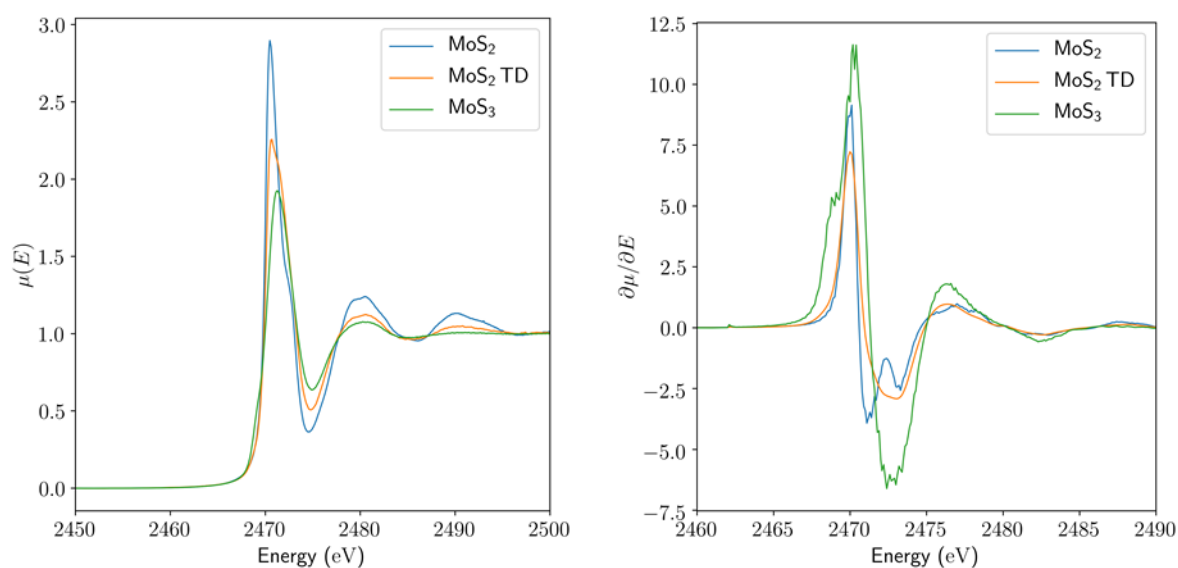


**Figure 14 - Left: XANES at the S K-edge of commercial MoS₂, MoS₂ TD and MoS₃. Right : First derivative of the spectra.**

To this day, there is no consensus in the literature regarding the structure of amorphous $MoS_3$. In particular, Hibble *et al.* proposed a linear structure,[53] but Weber *et al.* suggested instead that $MoS_3$ presents a 3D structure whose units are trinuclear $Mo_3S_9$ (see Figure 15).[17] More precisely, they propose units structurally identical to $[Mo_3S_{13}]^{2-}$ clusters that share terminal sulfur atoms. These terminal sulfur atoms can be substituted by chlorine

atoms upon addition of chlorohydric acid on $(NH_4)_2[Mo_3S_{13}]$, yielding $(NH_4)_2[Mo_3S_7Cl_6]$ (see Figure S3).[19–21] From XANES at the S K-edge (Figure 16), we confirm that sulfur is mainly present in the form of reduced sulfur species in our samples, since the absorption edge is located at 2470-2471 eV.
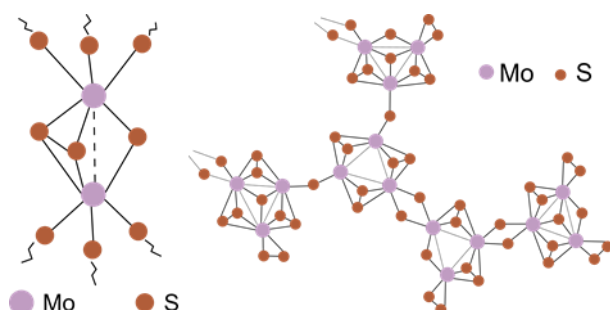


**Figure 15 - Proposed structures for amorphous MoS₃. Left : linear structure proposed by Hibble *et al.*,[54] right : tri-dimensional structure from Weber *et al.*[17]**
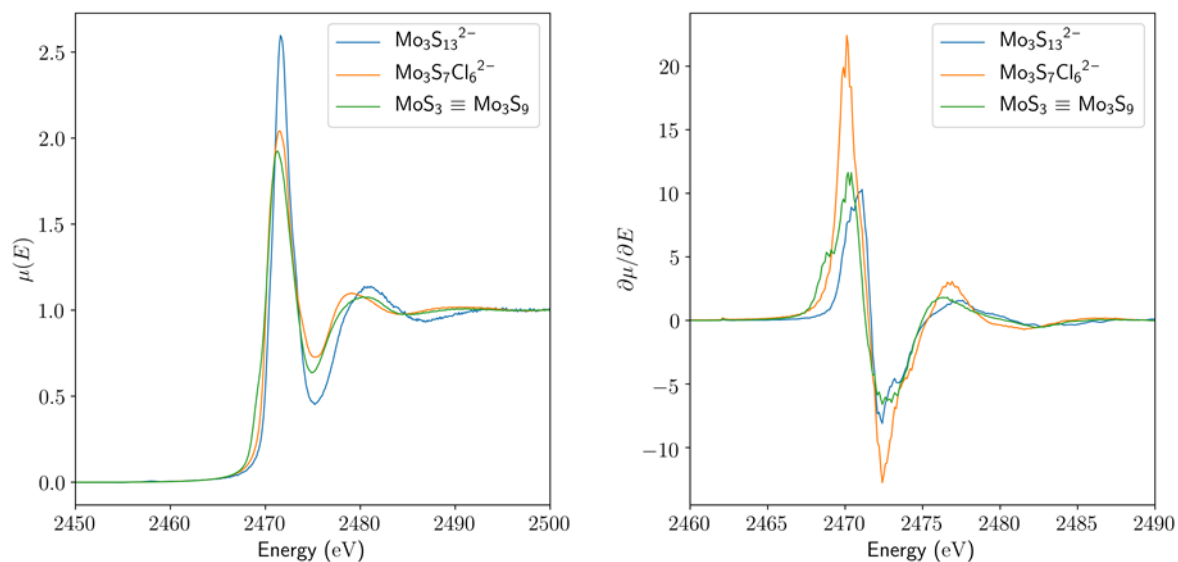


**Figure 16 - Left: XANES at the S K-edge of Mo₃Sₓ compounds. Right: First derivative of the spectra.**

Here, we measured the XAS signals of Mo at the $L_{2,3}$-edges for both $(NH_4)_2[Mo_3S_{13}]$ and $(NH_4)_2[Mo_3S_7Cl_6]$ tri-metallic clusters and we compare them to the XANES of $MoS_3$ (Figure 17). All three spectra are similar: the $L_3$-edge and the $L_2$-edge are located at *ca.* 2522.5 and 2627.3 eV, with an additional peak at 2532.5 eV. The second derivatives of the spectra are also similar: they exhibit a single feature large of *ca.* 2.2 eV (see also Table 3). Therefore, the spectrum of $MoS_3$ closely resembles the spectra of $[Mo_3S_{13}]^{2-}$ and $[Mo_3S_7Cl_6]^{2-}$, supporting the amorphous tri-dimensional environment proposed by Weber *et*

*al*. However, it seems that we cannot fully exclude the linear structure hypothesised by Hibble *et al.* To do so, we would need to record a linear compound of molybdenum sulfide to see if the XANES signal – in particular the second derivative of the data at Mo $L_{2,3}$-edges – would be different enough to close that discussion.
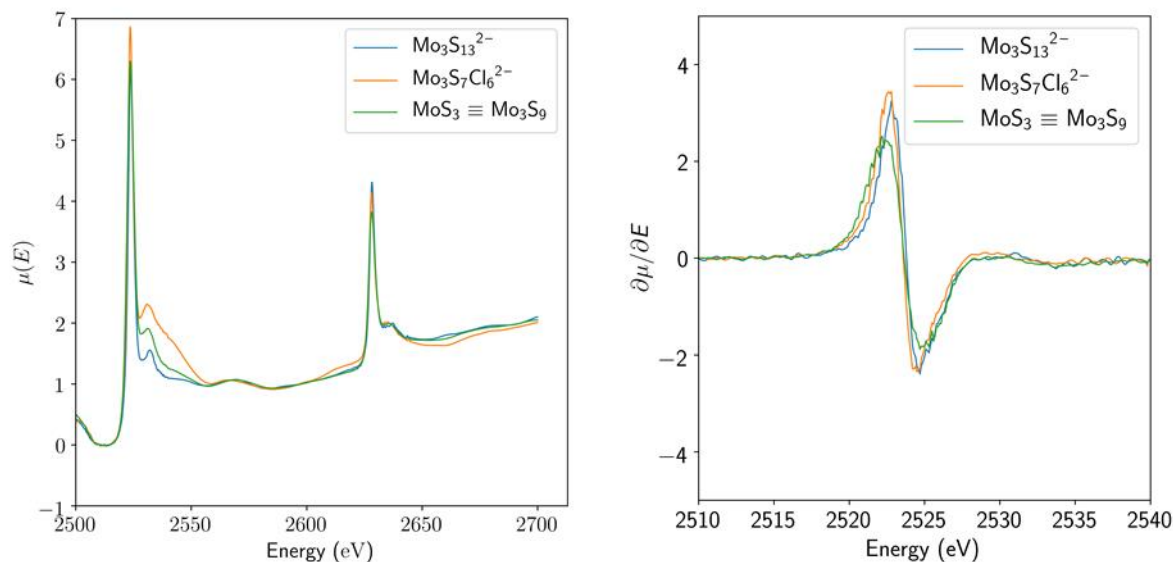


Figure 17 - Left: XANES of $Mo_3S_x$ compounds at the Mo $L_{2,3}$-edges. Right: first derivative of the Mo $L_3$-edge.

| Compound (formal redox state) | Position of the Mo $L_3$-edge (eV) | Position of the Mo $L_2$-edge (eV) | Position of the S K-edge (eV) |
|---|---|---|---|
| $MoS_2$ commercial | 2522.5 | 2627.1 | 2470.0 |
| $MoS_2$ TD | 2522.5 | 2627.1 | 2470.0 |
| $MoS_3$ | 2522.5 | 2627.0 | 2470.3 |
| $Mo_3S_{13}$ | 2522.8 | 2627.3 | 2470.0 |
| $Mo_3S_7Cl_6$ | 2522.8 | 2627.4 | 2470.3 |

Table 3 - Positions of the edges for the molybdenum sulfide compounds

## 4. Conclusion

To summarise, we proposed an empirical method to qualitatively interpret XANES at the Mo $L_{2,3}$-edges, based on selected Mo compounds with different geometries. The first-derivative of the spectrum (preferably at the $L_3$-edge) is better suited to study the redox state of Mo while the second derivative (preferably at the $L_2$-edge, because it is less sensitive to multiplet effects than the $L_3$-edge) is more appropriate to determine the geometry around Mo. Finally, we

compared the XANES of several molybdenum sulfide compounds with that of amorphous $MoS_3$ and propose a tridimensional structure similar to the one of $Mo_3S_{13}^{2-}$ and $Mo_3S_7Cl_6^{2-}$ clusters. We believe that these guidelines and the library of reference spectra provided will help interpret XAS data of Mo at the $L_{2,3}$-edges in future studies.

## Supporting Information

Additional XANES data. Scheme for the reaction of conversion of $[Mo_3S_{13}]^{2-}$. Supplementary file: experimental data of the spectra.

## References

(1)  Lauritsen, J. V.; Nyberg, M.; Nørskov, J. K.; Clausen, B. S.; Topsøe, H.; Lægsgaard, E.; Besenbacher, F. Hydrodesulfurization Reaction Pathways on MoS2 Nanoclusters Revealed by Scanning Tunneling Microscopy. *J. Catal.* **2004**, *224* (1), 94–106. https://doi.org/10.1016/j.jcat.2004.02.009.

(2)  Somorjai, G. A.; De Beer, V. H. J. Structure and Function of The Catalyst and The Promoter In Co—Mo Hydrodesuifurization Catalysts. *Catal. Rev.* **1989**, *31* (1–2), 1–41. https://doi.org/10.1080/01614948909351347.

(3)  Ressler, T.; Wienold, J.; Jentoft, R. E.; Neisius, T. Bulk Structural Investigation of the Reduction of MoO3 with Propene and the Oxidation of MoO2 with Oxygen. *J. Catal.* **2002**, *210* (1), 67–83. https://doi.org/https://doi.org/10.1006/jcat.2002.3659.

(4)  Bare, S. R.; Mitchell, G. E.; Maj, J. J.; Vrieland, G. E.; Gland, J. L. Local Site Symmetry of Dispersed Molybdenum Oxide Catalysts: XANES at the Mo L2,3-Edges. *J. Phys. Chem.* **1993**, *97* (22), 6048–6053. https://doi.org/10.1021/j100124a043.

(5)  Lede, E. J.; Requejo, F. G.; Pawelec, B.; Fierro, J. L. G. XANES Mo L-Edges and XPS Study of Mo Loaded in HY Zeolite. *J. Phys. Chem. B* **2002**, *106* (32), 7824–7831. https://doi.org/10.1021/jp014648p.

(6)  Appel, A. M.; DuBois, D. L.; Rakowski DuBois, M.; M. Appel, A.; L. DuBois, D.; Rakowski DuBois, M. Molybdenum−Sulfur Dimers as Electrocatalysts for the

Production of Hydrogen at Low Overpotentials. *J. Am. Chem. Soc.* **2005**, *127* (36), 12717–12726. https://doi.org/10.1021/ja054034o.

(7) Jaramillo, T. F.; Bonde, J.; Zhang, J.; Ooi, B.-L. L.; Andersson, K.; Ulstrup, J.; Chorkendorff, I.; F. Jaramillo, T.; Bonde, J.; Zhang, J.; et al. Hydrogen Evolution on Supported Incomplete Cubane-Type [Mo3S4]4+ Electrocatalysts. *J. Phys. Chem. C* **2008**, *112* (45), 17492–17498. https://doi.org/10.1021/jp802695e.

(8) Hinnemann, B.; Moses, P. G.; Bonde, J.; Jørgensen, K. P.; Nielsen, J. H.; Horch, S.; Chorkendorff, I.; Nørskov, J. K. Biomimetic Hydrogen Evolution: MoS2 Nanoparticles as Catalyst for Hydrogen Evolution. *J. Am. Chem. Soc.* **2005**, *127* (15), 5308–5309. https://doi.org/10.1021/ja0504690.

(9) Kibsgaard, J.; Jaramillo, T. F.; Besenbacher, F. Building an Appropriate Active-Site Motif into a Hydrogen-Evolution Catalyst with Thiomolybdate [Mo3S13]2- Clusters. *Nat. Chem.* **2014**, *6* (3), 248–253. https://doi.org/10.1038/nchem.1853.

(10) Tang, M. L.; Grauer, D. C.; Lassalle-Kaiser, B.; Yachandra, V. K.; Amirav, L.; Long, J. R.; Yano, J.; Alivisatos, A. P. Structural and Electronic Study of an Amorphous MoS3 Hydrogen-Generation Catalyst on a Quantum-Controlled Photosensitizer. *Angew. Chemie* **2011**, *123* (43), 10385–10389. https://doi.org/10.1002/ange.201104412.

(11) Merki, D.; Fierro, S.; Vrubel, H.; Hu, X. Amorphous Molybdenum Sulfide Films as Catalysts for Electrochemical Hydrogen Production in Water. *Chem. Sci.* **2011**, *2* (7), 1262–1267. https://doi.org/10.1039/c1sc00117e.

(12) Cramer, S. P.; Eccles, T. K.; Kutzler, F. W.; Hodgson, K. O.; Mortenson, L. E. Molybdenum X-Ray Absorption Edge Spectra. The Chemical State of Molybdenum in Nitrogenase. *J. Am. Chem. Soc.* **1976**, *98* (5), 1287–1288. https://doi.org/10.1021/ja00421a053.

(13) George, G. N.; Cleland, W. E.; Enemark, J. H.; Smith, B. E.; Kipke, C. A.; Roberts, S. A.; Cramer, S. P. L-Edge Spectroscopy of Molybdenum Compounds and Enzymes. *J. Am. Chem. Soc.* **1990**, *112* (7), 2541–2548. https://doi.org/10.1021/ja00163a010.

(14) Bjornsson, R.; Delgado-Jaime, M. U.; Lima, F. A.; Sippel, D.; Schlesier, J.; Weyhermüller, T.; Einsle, O.; Neese, F.; De Beer, S. Molybdenum L-Edge XAS Spectra of MoFe Nitrogenase. *Zeitschrift fur Anorg. und Allg. Chemie* **2015**, *641* (1), 65–71. https://doi.org/10.1002/zaac.201400446.

(15) Vantelon, D.; Trcera, N.; Roy, D.; Moreno, T.; Mailly, D.; Guilet, S.; Metchalkov, E.; Delmotte, F.; Lassalle, B.; Lagarde, P.; et al. The LUCIA Beamline at SOLEIL. *J. Synchrotron Radiat.* **2016**, *23* (2), 635–640. https://doi.org/10.1107/S1600577516000746.

(16) Thomas, R.; Kas, J.; Glatzel, P.; Al Samarai, M.; de Groot, F. M. F.; Alonso Mori, R.; Kavčič, M.; Zitnik, M.; Bucar, K.; Rehr, J. J.; et al. Resonant Inelastic X-Ray Scattering of Molybdenum Oxides and Sulfides. *J. Phys. Chem. C* **2015**, *119* (5), 150126100226006. https://doi.org/10.1021/jp509376q.

(17) Weber, T.; Muijsers, J. C.; Niemantsverdriet, J. W. Structure of Amorphous MoS3. *J. Phys. Chem.* **1995**, *99* (22), 9194–9200. https://doi.org/10.1021/j100022a037.

(18) Walton, R. I.; Dent, A. J.; Hibble, S. J. In Situ Investigation of the Thermal Decomposition of Ammonium Tetrathiomolybdate Using Combined Time-Resolved X-Ray Absorption Spectroscopy and X-Ray Diffraction. *Chem. Mater.* **1998**, *10* (11), 3737–3745. https://doi.org/10.1021/cm980716h.

(19)     Müller, A.; Jostes, R.; Jaegermann, W.; Bhattacharyya, R. Spectroscopic Investigation on the Molecular and Electronic Structure of [Mo3S13]2-, a Discrete Binary Transition Metal Sulfur Cluster. *Inorganica Chim. Acta* **1980**, *41* (C), 259–263. https://doi.org/10.1016/S0020-1693(00)88466-2.

(20)     Müller, A.; Krickemeyer, E.; Hadjikyriacou, A.; Coucouvanis, D. Molybdenum-Sulfur Clusters. In *Inorganic Syntheses Volume 27*; Ginsberg, A. P., Ed.; John Wiley & Sons, Inc., 1990; pp 47–51. https://doi.org/10.1002/9780470132586.ch9.

(21)     Hédoire, C. E.; Cadot, E.; Villain, F.; Davidson, A.; Louis, C.; Breysse, M. Preparation and Characterization of Molybdenum Sulfide Supported on β-Zeolites Obtained from [Mo3S4(H2O)9]4+ Precursor. *Appl. Catal. A Gen.* **2006**, *306*, 165–174. https://doi.org/10.1016/j.apcata.2006.03.045.

(22)     Larson, M. L.; Moore, F. W. Synthesis and Properties of Molybdenum(III) Acetylacetonate. *Inorg. Chem.* **1962**, *1* (4), 856–859. https://doi.org/10.1021/ic50004a030.

(23)     De Groot, F. M. F.; Hu, Z. W.; Lopez, M. F.; Kaindl, G.; Guillot, F.; Tronc, M. Differences between L3 and L2 X-Ray Absorption Spectra of Transition Metal Compounds. *J. Chem. Phys.* **1994**, *101* (8), 6570–6576. https://doi.org/10.1063/1.468351.

(24)     Hodgson, K. O.; Hedman, B.; Penner-Hahn, J. E. Molybdenum LII,III Edge Studies. In *EXAFS and Near Edge Structure III*; Hodgson, K. O., Hedman, B., Penner-Hahn, J. E., Eds.; Springer-Verlag: Stanford, 1984; pp 64–66.

(25)     Evans, J.; Mosselmans, J. F. W. L-Edge Studies on Molybdenum. *J. Phys. Chem.* **1991**, *95* (24), 9673–9676. https://doi.org/10.1021/j100177a015.

(26)     Thole, B. T.; Van Der Laan, G. Branching Ratio in X-Ray Absorption Spectroscopy. *Phys. Rev. B* **1988**, *38* (5), 3158–3171. https://doi.org/10.1103/PhysRevB.38.3158.

(27)     de Groot, F. M. F. Differences between L3 and L2 X-Ray Absorption Spectra. *Phys. B Phys. Condens. Matter* **1995**, *208–209* (C), 15–18. https://doi.org/10.1016/0921-4526(94)00817-F.

(28)     Ikeno, H.; Tanaka, I.; Miyamae, T.; Mishima, T.; Adachi, H.; Ogasawara, K. First Principles Calculation of Fe L 2,3-Edge X-Ray Absorption near Edge Structures of Iron Oxides. *Mater. Trans.* **2004**, *45* (5), 1414–1418. https://doi.org/10.2320/matertrans.45.1414.

(29)     Bearden, J. A.; Burr, A. F. Reevaluation of X-Ray Atomic Energy Levels. *Rev. Mod. Phys.* **1967**, *39* (1), 125–142. https://doi.org/10.1103/RevModPhys.39.125.

(30)     Aritani, H.; Tanaka, T.; Funabiki, T.; Yoshida, S.; Eda, K.; Sotani, N.; Kudo, M.; Hasegawa, S. Study of the Local Structure of Molybdenum−Magnesium Binary Oxides by Means of Mo L 3 -Edge XANES and UV−Vis Spectroscopy. *J. Phys. Chem.* **1996**, *100* (50), 19495–19501. https://doi.org/10.1021/jp9615464.

(31)     Brandt, B. G. On the Crystal Structures of MoO2 and MoO3.2H2O: An Account of Computer Programming and Structure Refinement. In *Chemical Communications University of Stockholm Volume 9*; 1971.

(32)     Kihlborg, L. Least Squares Refinement of the Crystal Struc-Ture of Molybdenum Trioxide. *Ark. Kemi* **1963**, *21*, 357–364.

(33)     Evans, H. T.; Gatehouse, B. M.; Leverett, P. Crystal Structure of the Heptamolybdate(VI) (Paramolybdate) Ion, [Mo7O24]6-, in the Ammonium and

Potassium Tetrahydrate Salts. *J. Chem. Soc. Dalt. Trans.* **1975**, No. 6, 505–514. https://doi.org/10.1039/DT9750000505.

(34) Allmann, R.; Kjekshus, A.; Valde, G.; Andresen, A. F.; Sandström, M. About the Space Group of H3Mo12PO40(H2O)29-31; a Discussion. *Acta Chem. Scand.* **1976**, *30a*, 152–152. https://doi.org/10.3891/acta.chem.scand.30a-0152.

(35) Lu, Y. K.; Li, Y. P.; Yang, L. Y.; Wang, W. H.; Pan, Y.; Yan, W. F.; Liu, Y. Q. Modified Polyoxometalate: A Novel Monocapped Bi-Supporting and Reduced α-Keggin Structure {PMo12O40[Cu(2,2′-Bpy)]}[Cu(2,2′-Bpy)(En)(H2O)]2. *Acta Crystallogr. Sect. C Struct. Chem.* **2019**, *75*, 1344–1352. https://doi.org/10.1107/S2053229619011999.

(36) Xu, Y.; Xu, J.-Q.; Yang, G.-Y.; Yang, G.-D.; Xing, Y.; Lin, Y.-H.; Jia, H.-Q. (NH 4 ) 3 [PMo 12 O 40 ].21H 2 O. *Acta Crystallogr. Sect. C Cryst. Struct. Commun.* **1998**, *54* (1), 9–11. https://doi.org/10.1107/S0108270197011128.

(37) Hillebrecht, H.; Schmidt, P. J.; Rotter, H. W.; Thiele, G.; Zönnchen, P.; Bengel, H.; Cantow, H. J.; Magonov, S. N.; Whangbo, M. H. Structural and Scanning Microscopy Studies of Layered Compounds MCl3 (M = Mo, Ru, Cr) and MOCl2 (M = V, Nb, Mo, Ru, Os). *J. Alloys Compd.* **1997**, *246* (1–2), 70–79. https://doi.org/10.1016/S0925-8388(96)02465-6.

(38) Sands, D. E.; Zalkin, A. The Crystal Structure of MoCl5. *Acta Crystallogr.* **1959**, *12* (10), 723–726. https://doi.org/10.1107/s0365110x59002146.

(39) Krasochka, O. N.; Sokolova, Y. A.; Atovmyan, L. O. Crystal and Molecular Structures of Molybdenum Bis-Acetylacetonate, MoO2(C5H7O2)2. *J. Struct. Chem.* **1975**, *16* (4), 648–650. https://doi.org/10.1007/BF00754060.

(40) Ledneva, A. Y.; Artemkina, S. B.; Piryazev, D. A.; Fedorov, V. E. Structure and Thermal Properties of the Molybdenum Complex Mo(Acac)3. *J. Struct. Chem.* **2015**, *56* (5), 1021–1023. https://doi.org/10.1134/S0022476615050315.

(41) Gould, R. O.; Barker, J.; Kilner, M. Gauche Conformer of Bis[Tricarbonyl(Cyclopentadienyl)Molybdenum]. *Acta Crystallogr. Sect. C Cryst. Struct. Commun.* **1988**, *44* (3), 461–463. https://doi.org/10.1107/s0108270187012137.

(42) Cotton, F. A.; Norman, J. G. MOLYBDENUM(II) TRIFLUORO ACETATE DIMER. *J. Coord. Chem.* **1972**, *1* (3), 161–171. https://doi.org/10.1080/00958977208070758.

(43) Hillenbrand, J.; van Gastel, M.; Bill, E.; Neese, F.; Fürstner, A. Isolation of a Homoleptic Non-Oxo Mo(V) Alkoxide Complex: Synthesis, Structure, and Electronic Properties of Penta-Tert-Butoxymolybdenum. *J. Am. Chem. Soc.* **2020**, *142* (38), 16392–16402. https://doi.org/10.1021/jacs.0c07073.

(44) Cotton, F. A.; DeBoer, B. G.; LaPrade, M. D.; Pipal, J. R.; Ucko, D. A. The Crystal and Molecular Structures of Dichromium Tetraacetate Dihydrate and Dirhodium Tetraacetate Dihydrate. *Acta Crystallogr. Sect. B Struct. Crystallogr. Cryst. Chem.* **1971**, *27* (8), 1664–1671. https://doi.org/10.1107/s0567740871004527.

(45) Lawton, D.; Mason, R. The Molecular Structure of Molybdenum(II) Acetate [8]. *J. Am. Chem. Soc.* **1965**, *87* (4), 921–922. https://doi.org/10.1021/ja01082a046.

(46) Rochet, A.; Baubet, B.; Moizan, V.; Devers, E.; Hugon, A.; Pichon, C.; Payen, E.; Briois, V. Intermediate Species Revealed during Sulfidation of Bimetallic Hydrotreating Catalyst: A Multivariate Analysis of Combined Time-Resolved Spectroscopies. *J. Phys. Chem. C* **2017**, *121* (34), 18544–18556. https://doi.org/10.1021/acs.jpcc.7b03735.

(47) Lassalle-Kaiser, B.; Merki, D.; Vrubel, H.; Gul, S.; Yachandra, V. K.; Hu, X.; Yano, J. Evidence from in Situ X-Ray Absorption Spectroscopy for the Involvement of Terminal Disulfide in the Reduction of Protons by an Amorphous Molybdenum Sulfide Electrocatalyst. *J. Am. Chem. Soc.* **2015**, *137* (1), 314–321. https://doi.org/10.1021/ja510328m.

(48) Parija, A.; Choi, Y. H.; Liu, Z.; Andrews, J. L.; De Jesus, L. R.; Fakra, S. C.; Al-Hashimi, M.; Batteas, J. D.; Prendergast, D.; Banerjee, S. Mapping Catalytically Relevant Edge Electronic States of MoS2. *ACS Cent. Sci.* **2018**, *4* (4), 493–503. https://doi.org/10.1021/acscentsci.8b00042.

(49) Merki, D.; Vrubel, H.; Rovelli, L.; Fierro, S.; Hu, X. Fe, Co, and Ni Ions Promote the Catalytic Activity of Amorphous Molybdenum Sulfide Films for Hydrogen Evolution. *Chem. Sci.* **2012**, *3* (8), 2515–2525. https://doi.org/10.1039/c2sc20539d.

(50) Vrubel, H.; Merki, D.; Hu, X. Hydrogen Evolution Catalyzed by MoS3 and MoS2 Particles. *Energy Environ. Sci.* **2012**, *5* (3), 6136–6144. https://doi.org/10.1039/c2ee02835b.

(51) Vrubel, H.; Hu, X. Growth and Activation of an Amorphous Molybdenum Sulfide Hydrogen Evolving Catalyst. *ACS Catal.* **2013**, *3* (9), 2002–2011. https://doi.org/10.1021/cs400441u.

(52) Larquet, C.; Nguyen, A. M.; Ávila-Gutiérrez, M.; Tinat, L.; Lassalle-Kaiser, B.; Gallet, J. J.; Bournel, F.; Gauzzi, A.; Sanchez, C.; Carenco, S. Synthesis of Ce2O2S and Gd2(1-y)Ce2yO2S Nanoparticles and Reactivity from in Situ X-Ray Absorption Spectroscopy and X-Ray Photoelectron Spectroscopy. *Inorg. Chem.* **2017**, *56* (22), 14227–14236. https://doi.org/10.1021/acs.inorgchem.7b02336.

(53) Hibble, S. J.; Rice, D. A.; Pickup, D. M.; Beer, M. P. Mo K-Edge EXAFS and S K-Edge Absorption Studies of the Amorphous Molybdenum Sulfides MoS4.7, MoS3, and MoS3·nH2O (n ~ 2). *Inorg. Chem.* **1995**, *34* (21), 5109–5113. https://doi.org/10.1021/ic00125a006.

(54) Hibble, S. J.; Rice, D. A.; Pickup, D. M.; Beer, M. P. Mo K-Edge EXAFS and S K-Edge Absorption Studies of the Amorphous Molybdenum Sulfides MoS4.7, MoS3, and MoS3·nH2O (n ~ 2). *Inorg. Chem.* **1995**, *34* (21), 5109–5113. https://doi.org/10.1021/ic00125a006.

# TOC Graphic